CHINESE JOURNAL OF PHYSICS VOL. 51, NO. 4 August 2013

Thermoelectric Properties of an Individual $Bi_{1.75}Sb_{0.25}Te_{2.02}$ Nanowire

Ping-Chung Lee,[1,2,*] Hong-Chi Chen,[3] Chuan-Ming Tseng,[3] Wei-Chiao Lai,[3] Chih-Hao Lee,[1] Chia-Seng Chang,[3] and Yang-Yuan Chen[3,†]

[1]*Department of Engineering and System Science, National TsingHua University, Hsinchu, Taiwan, Republic of China*
[2]*Nano Science and Technology Program, Taiwan International Graduate Program, Academia Sinica, Nankang, Taipei, Taiwan, Republic of China*
[3]*Institute of Physics, Academia Sinica, Nankang, Taipei, Taiwan, Republic of China*

(Received March 26, 2013; Revised April 18, 2013)

A single crystalline $Bi_{1.75}Sb_{0.25}Te_{2.02}$ nanowire of 250 nm in diameter was grown from a $Bi_{1.5}Sb_{0.5}Te_3$ film via the thermal annealing method. The growth direction along [110] and the stoichiometric composition of $Bi_{1.75}Sb_{0.25}Te_{2.02}$ for this nanowire were confirmed by the TEM results, and the layered morphology of the a-b plane was clearly observed by AFM and SEM. The self-heating 3ω technique was employed to characterize the thermal conductivity of this nanowire. The result shows that the thermal conductivity increases from 0.5 W/m-K at 10 K to 1.2 W/m-K at 120 K, then followed by a slight increase to 1.4 W/m-K at 300 K. It is observed that the low-temperature thermal conductivity of bismuth-antimony-telluride nanowire at 20 K is about six times lower than that of its bulk counterpart. The enormous reduction on thermal conductivity is mainly attributed to the enhanced phonon-boundary scattering of the nanometer size effect. In addition, the electrical resistivity and Seebeck coefficient were also simultaneously measured by the heater and electrodes built in the platform.

DOI: PACS numbers: 73.63.Nm, 72.15.Jf

I. INTRODUCTION

Bismuth-antimony-tellurium based compounds are well-known thermoelectric (TE) materials with the maximum value of figure of merit, ZT $\sim$ 1.2, around room temperature, and have thus attracted many research groups devoted in improving their heat and electricity conversion efficiency represented by the dimensionless ZT value. Guo *et al.* studied the pressure effect on the power factor of $Bi_{1.5}Sb_{0.5}Te_3$ alloys prepared by the high-pressure high-temperature (HPHT) method, and showed an increment in the Seebeck coefficient with an increase of synthesis pressure [1]. Liu *et al.* demonstrated the mechanical alloying followed by pulse discharge sintering (MA-PDS) on various antimony contents in $(Bi_{1-x}Sb_x)_2Te_3$ and revealed ZT close to 1 at room temperature [2]. The nanocomposite ap-

*Electronic address: iamplex@phys.sinica.edu.tw
†Electronic address: cheny2@phys.sinica.edu.tw

proach adopted by Fan *et al.* was able to increase the ZT to 1.4 for p-type $Bi_{0.4}Sb_{1.6}Te_3$ [3]. Meanwhile, one dimensional TE materials were predicted to potentially enhance the value of ZT, first by theorists [4, 5], and later the remarkable enhancement in the ZT of silicon nanowires was demonstrated experimentally [6]. Going one step further, surface modification of Si nanowires was employed to reduce their thermal conductivity so that the ZT value can climb even higher [7].

Many studies also investigated the unusual physical properties of bismuth-tellurium based nanowires. Xiao *et al.* measured the electro-transport property of $(Bi_{1-x}Sb_x)_2Te_3$ nanowires on the template and found that their thermal activation energy was dependent on the nanowire's composition [8]. Furthermore, ZT enhancement to ~ 0.9 at 350 K due to reduction of the thermal conductivity has been observed in a Bi_2Te_3 nanowire array, fabricated by the anodized aluminum matrix (AAM) template [9]. In order to unveil the intrinsic physical contents of the size effect on TE materials, the measurement of an individual nanowire without interference from either the matrix or external contacts becomes imperative [10, 11]. In this work, we have studied the TE, stoichiometric, and crystalline properties of a single $Bi_{1.75}Sb_{0.25}Te_{2.02}$ nanowire grown by the thermal annealing method [12, 13].

II. EXPERIMENTAL DETAILS

The bismuth antimony telluride nanowires were synthesized by the thermal annealing method, which is a practical method for growing the nanowires with high aspect ratio and high crystallinity. Bi_2Te_3 and Sb_2Te_3 powders were first mixed with a specific ratio and heated up to 750 °C in a sealed quartz tube. After three hours of annealing, the melted compound was slowly cooled down to room temperature and cut to a disk shape to serve as the target for the pulsed laser deposition (PLD). The structure and composition of the target were confirmed by X-ray diffraction (XRD) as the hexagonal structure and by energy-dispersive X-ray spectroscopy (EDX) with composition of $Bi_{1.5}Sb_{0.5}Te_3$, respectively. $Bi_{1.5}Sb_{0.5}Te_3$ thin films were prepared on SiO_2/Si substrates by deposition using the ArF excimer laser (Lambda Physik LPXpro) with a pulse energy of 200 mJ and frequency of 10 Hz. The deposited Films were then sealed in a quartz tube for post annealing at 350 °C for 5 days. The highly crystalline nanowires were grown through release of the stress, which originated from the mismatch in the thermal expansion between the $Bi_{1.5}Sb_{0.5}Te_3$ film and the SiO_2/Si substrate [12]. Scanning electron microscopy (SEM) images showed that the diameters of the bismuth antimony telluride nanowires varied from a few tens to several hundreds of nanometers, with the typical length of several tens of micrometers. In order to measure the physical properties of an individual nanowire, one bismuth antimony telluride nanowire was selected from the substrate and transferred to the platform (Fig. 1a) by a tungsten tip under an optical microscope. To ensure solid electrical and thermal contacts between the nanowire and the electrodes, additional platinum was deposited on the contacts by a focused ion beam (Fig. 1b). The layered morphology of this nanowire was revealed by the SEM image, as shown in Figure 1c. The cross-sectional profile of this nanowire was measured by an atomic force microscope (AFM) and the result indicates that

the width and thickness of this nanowire are 890 and 250 nm, respectively.

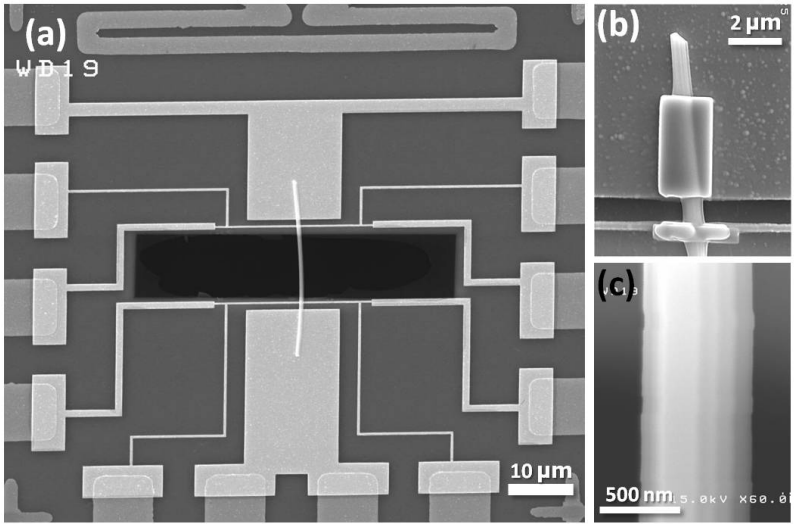

FIG. 1: (a) The SEM image of the measurement platform with an individual nanowire suspended on the open window. (b) The SEM image of the contact point after platinum deposition. (c) The layer structure observed by the SEM image of the nanowire.

Thermal conductivity measurement was performed by the method of self-heating 3ω technique [14–17] on the nanowire that was suspended in vacuum. To hold the suspended nanowire, the silicon wafer was wet-etched to open a window, and this was followed by photolithography to define the electrodes. The heater, resistance temperature detector (RTD), and current leads of Au/Cr were fabricated by an e-beam writer and thermal evaporation (Fig. 1a) for the measurements of the electromotive force (EMF: ΔV) and temperature gradient on the nanowire. The four-point probe method for resistivity ρ measurement can also be performed by the deposited electrodes.

III. RESULTS AND DISCUSSION

The selected area electron diffraction (SAED) pattern (Fig. 2a) taken from the $Bi_{1.75}Sb_{0.25}Te_{2.02}$ nanowire confirms its single crystallinity of the hexagonal symmetry and its growth direction in [110], which is similar to the tellurium based nanowires grown by the thermal annealing method [13]. The STEM-EDX mapping results show that the bismuth, antimony, and tellurium are uniformly distributed in the nanowire (Fig. 2b–2d). The STEM-EDX point scan indicates that the stoichiometric composition of this nanowire is $Bi_{1.75}Sb_{0.25}Te_{2.02}$.

To characterize the TE properties of this nanowire, the Seebeck coefficient α was measured first. The inset of Figure 3 depicts the linear fit of the temperature gradient dependence of the nanowire's EMF at 245 K. The slope of the linear fit represents the

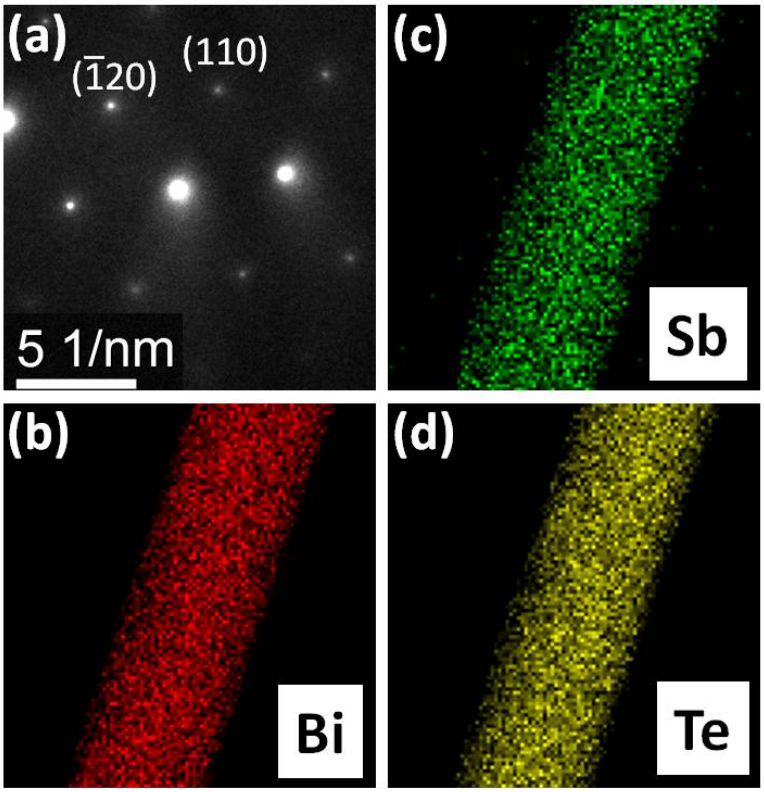

FIG. 2: (a) The SAED pattern of the nanowire. The STEM mapping result indicates that bismuth (b), tellurium (c), and antimony (d) are all uniformly distributed in the nanowire.

Seebeck coefficient at this temperature. Figure 3 displays the Seebeck coefficient over the temperature range of 150–300 K. The result shows that the $Bi_{1.75}Sb_{0.25}Te_{2.02}$ nanowire is an n-type TE material with Seebeck coefficient around -60 μV/K at 300 K, which is close to the value obtained on the rapidly quenched $Bi_{1.4}Sb_{0.6}Te_3$ foils [18]. The trend on the temperature dependence of the resistivity ρ exhibits the metallic behavior of this nanowire (Fig. 4). The temperature dependence of the calculated power factor α^2/ρ is shown in the inset of Figure 4 with a maximum of $\sim$ 0.4 mW/m-K^2 at room temperature. This value is the same as that of the rapidly quenched $Bi_{1.4}Sb_{0.6}Te_3$ foils at room temperature, but relatively lower than that of other bismuth-antimony-tellurium based compounds. To further improve the power factor, which is typically optimized as a function of carrier concentration, additional doping or post annealing of the nanowire can be applied.

The thermal conductivity measured by the self-heating 3ω method in the temperature range of 10–300 K is shown in Figure 5. The 3ω signal can be expressed as

$$V_{3\omega} \approx \frac{4I^3LRR'}{\pi^4 KS\sqrt{1+(2\omega\gamma)^2}},$$

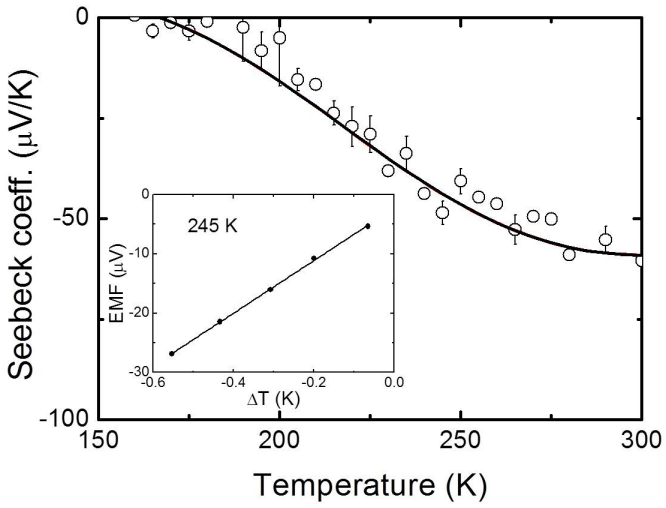

FIG. 3: Temperature dependence of the Seebeck coefficient. Inset: the temperature gradient dependence of the EMF for the nanowire at 245 K.

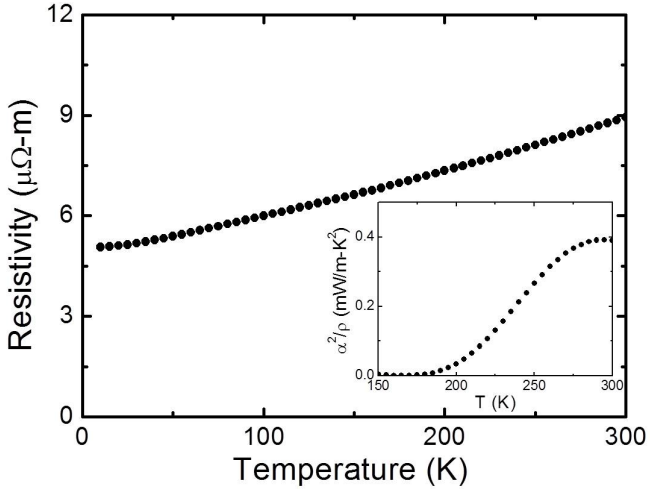

FIG. 4: Temperature dependence of the electrical resistivity. Inset: the calculated power factor for the nanowire.

where I and ω are the amplitude and frequency of the alternating current applied on the nanowire, R and R' are the resistance and derivative of resistance at the corresponding temperature, K is the thermal conductivity, S is the cross section area, and γ is the characteristic thermal time constant [14]. Each data point in Figure 5 is obtained through

fitting the frequency dependence of $V_{3\omega}$ with the relation of $V_{3\omega} \propto 1\Big/\sqrt{1+(2\omega\gamma)^2}$, the inset (a) of Figure 5 shows the fitting result at 290 K. The thermal conductivity K of the nanowire can be derived from the intercept $V_{3\omega} \approx \frac{4I^3LRR'}{\pi^4 KS}$ $(\omega\gamma \to 0)$ of the fitting value at a certain temperature. The frequency dependence of the phase angle $\tan(180-\varphi) \approx 2\omega\gamma$ is shown in the inset (b) of Figure 5, $\tan(180-\varphi) \propto \omega$ and $0 < 2\omega\gamma < 4$ indicates the usable frequency range for the frequency dependent measurements.

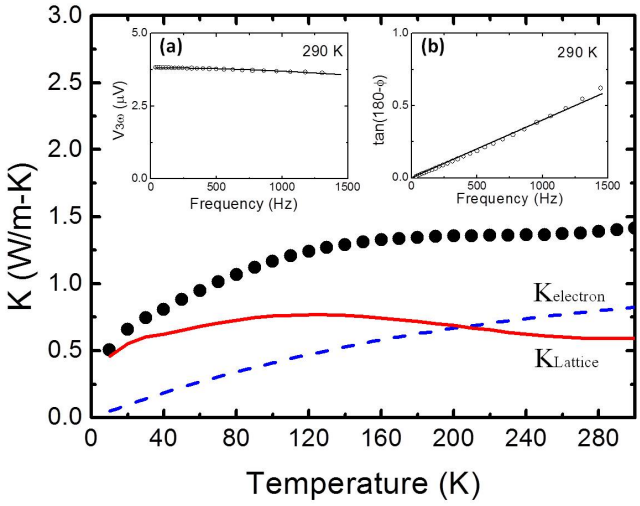

FIG. 5: Temperature dependence of thermal conductivity represented by solid circles. The electron thermal conductivity estimated by the Wiedemann-Franz law is represented by the dashed line, and the lattice thermal conductivity is represented by the solid line. Inset (a): the frequency dependence of the 3ω signal and the theoretical simulation (solid line) at 290 K. (b): the frequency dependence of the phase angle $\tan(180-\phi)$ for the measurement at 290 K.

The thermal conductivity of this bismuth-antimony-telluride nanowire in the low temperature region is about six times smaller than that of its bulk counterpart. The thermal conductivity contributed by the conduction electrons K_{electron} was estimated by the Wiedemann-Franz law (the dashed line in Figure 5). The resulting lattice thermal conductivity K_{Lattice} (the solid line in Figure 5) was then obtained by subtracting the electronic contribution K_{electron} from the total thermal conductivity. The maximum of the lattice thermal conductivity K_{Lattice} shifted to 120 K, which is about 100 K higher than that of bulk $Bi_{0.5}Sb_{1.5}Te_3$. These features of the K_{Lattice} maximum shifting and the magnitude suppression are attributed to the enhanced phonon-boundary scatterings, which have been commonly observed in various nanowire/nano-ribbon systems [17, 19]. In the high temperature region, since the phonon mean free path is much smaller than the geometric size of the nanowire, no significant change in thermal conductivity was observed [20].

In this work, a $Bi_{1.75}Sb_{0.25}Te_{2.02}$ nanowire grown by the thermal annealing method

has been characterized by TEM, SEM, and AFM. The results show that this nanowire was grown in the [110] direction with the stoichiometric composition of $Bi_{1.75}Sb_{0.25}Te_{2.02}$, and the layer structure morphology in the a-b plane was clearly observed. Furthermore, the three thermoelectric related properties of this nanowire, i.e., electrical resistivity, thermal conductivity, and Seebeck coefficient, have been successfully measured. The shift of the lattice thermal conductivity maximum and the magnitude suppression were observed and could be attributed to the enhanced phonon-boundary scatterings. Our experimental setup provides a platform to measure the TE properties including structural and compositional analyses on an individual nanowire. All measurements carried out on the same nanowire would prevent the possible errors from various parameters measured from different specimens, especially for those physical properties exhibiting strong sample dependence, and thus render a more accurate assessment of the resulting ZT value.

Acknowledgements

We would like to thank the NanoCore, the Core Facilities for Nanoscience and Nano technology at Academia Sinica in Taiwan, and the technical assistance from Pai-Chia Kuo. This work was supported by Academia Sinica and National Science Council, Taiwan, Republic of China, under Grant No. NSC100-2112-M-001-019-MY3.

References

[1] T. S. Oh, D.-B. Hyun, and N. V. Kolomoets, Scripta Mater. **42**, 849 (2000).
[2] L. Xue-Dong and Y.-H. Park, Mater. Trans. **43**, 681 (2002).
[3] S. Fan *et al.*, Appl. Phys. Lett. **96**, 182104 (2010). doi: 10.1063/1.2917705
[4] L. D. Hicks and M. S. Dresselhaus, Phys. Rev. B **47**, 16631 (1993). doi: 10.1103/PhysRevB.47.16631
[5] Y.-M. Lin, X. Sun, and M. S. Dresselhaus, Phys. Rev. B **62**, 4610 (2000). doi: 10.1103/PhysRevB.62.4610
[6] A. I. Boukai *et al.*, Nature **451**, 168 (2008). doi: 10.1038/nature06458
[7] A. I. Hochbaum, R. Chen, R. D. Delgado, W. Liang, E. C. Garnett *et al.*, Nature **451**, 163 (2008). doi: 10.1038/nature06381
[8] F. Xiao, B. Yoo, K.-H. Lee, and N. V Myung, Nanotechnology **18**, 335203 (2007). doi: 10.1088/0957-4484/18/33/335203
[9] C.-L. Chen, Y.-Y. Chen, S.-J. Lin, J. C. Ho, P.-C. Lee *et al.*, J. Phys. Chem. C **114**, 3385 (2010). doi: 10.1021/jp909926z
[10] A. Mavrokefalos *et al.*, J. Appl. Phys. **105**, 104318 (2009). doi: 10.1063/1.3133145
[11] K.-M. Lee, S.-K. Lee, and T.-Y. Choi, Appl. Phys. A **106**, 955 (2012). doi: s00339-011-6718-0
[12] J. Ham, W. Shim, D. H. Kim, S. Lee, J. Roh *et al.*, Nano Lett. **9**, 2867 (2009). doi: 10.1021/nl9010518
[13] W. Shim *et al.*, Nano Lett. **9**, 18 (2008). doi: 10.1021/nl8016829
[14] L. Lu, W. Yi, and D. L. Zhang, Rev. Sci. Instrum. **72**, 2996 (2001). doi: 10.1063/1.1378340
[15] T. Y. Choi, D. Poulikakos, J. Tharian, and U. Sennhauser, Appl. Phys. Lett. **87**, 013108 (2005).

doi: 10.1063/1.1957118
[16] M. N. Ou *et al.*, Appl. Phys. Lett. **92**, 063101 (2008). doi: 10.1063/1.2839572
[17] G. Li, D. Liang, R. L. J. Qiu, and X. P. A. Gao, Appl. Phys. Lett. **102**, 043104 (2013). doi: 10.1063/1.4789530
[18] E. L. Kukharenko and V. G. Shepelevich, Inorg. Mater.+ **36**, 134 (2000).
[19] D. Li *et al.*, Appl. Phys. Lett. **83**, 2934 (2003). doi: 10.1063/1.1616981
[20] T. Caillat, M. Carle, P. Pierrat, H. Scherrer, and S. Scherrer, J. Phys. Chem. Solids **53**, 1121 (1992). doi: 10.1016/0022-3697(92)90087-T